

## Estimating phytoplankton biomass in coastal waters of Alaska using airborne remote sensing

Martín A. Montes-Hugo<sup>a,\*</sup>, Kendall Carder<sup>a</sup>, Robert J. Foy<sup>b</sup>,  
Jennifer Cannizzaro<sup>a</sup>, Evelyn Brown<sup>c</sup>, Scott Pegau<sup>d</sup>

<sup>a</sup> EOS Lab, College of Marine Science, University of South Florida, 140 7th Ave S, St. Petersburg, FL 33701, USA

<sup>b</sup> Fishery Industrial Technology Center, School of Fisheries and Ocean Sciences, University of Alaska Fairbanks, AK 99615-7401, USA

<sup>c</sup> Institute of Marine Science, University of Alaska Fairbanks, School of Fisheries and Ocean Sciences, Fairbanks, AK 99775-7220, USA

<sup>d</sup> Kachemak Bay Research Reserve, Homer, NOAA, AK 99603, United States

Received 12 May 2005; received in revised form 16 July 2005; accepted 27 August 2005

### Abstract

Empirical airborne remote-sensing relationships were examined to estimate chlorophyll *a* concentration in the first optical depth ( $\text{chl}_{\text{FOD}}$ ) of coastal waters of Afognak/Kodiak Islands during July–August 2002. Band-ratio and spectral-curvature models were tested using satellite remote-sensing reflectance ( $R_{\text{rs}}(\lambda)$ ) measurements. Additional shipboard and airborne  $R_{\text{rs}}(\lambda)$  data were also analysed to evaluate consistency of proposed  $\text{chl}_{\text{FOD}}-R_{\text{rs}}(\lambda)$  relationships. Validation of chlorophyll algorithms was performed using data collected in the northern-part of the Gulf of Alaska and Bering Sea during 1996, 2002, and 2003 cruises. Likewise, oceanographic conditions during the surveys were typified to interpret variability of  $\text{chl}_{\text{FOD}}$  fields. The SeaWiFS band-ratio algorithm OC2d was the most sensitive  $R_{\text{rs}}$  combination ( $R_{\text{rs}}(509)/R_{\text{rs}}(553)$ ) to detect  $\text{chl}_{\text{FOD}}$  variability. Conversely, OC2a ( $R_{\text{rs}}(412)/R_{\text{rs}}(553)$ ) had the lowest performance to derive  $\text{chl}_{\text{FOD}}$  values. No valid statistical regressions were established for spectral–curvature relationships in the blue spectrum (<500 nm). Fertile waters (>5  $\text{mg m}^{-3}$ ) were preferentially located over shallow banks (~50 m) and at the entrance of the bays. The approach used in this study to derive  $\text{chl}_{\text{FOD}}$  values could be universal for Alaskan coastal waters. However,  $\text{chl}_{\text{FOD}}-R_{\text{rs}}(\lambda)$  relationships must be calibrated locally for a given season.

© 2005 Elsevier Inc. All rights reserved.

**Keywords:** Chlorophyll *a* concentration; Phytoplankton pigments; Productivity; Airborne surveys; Satellite images; SeaWiFS; Remote sensing; Gulf of Alaska; Coastal waters

### 1. Introduction

In the last five years, the northern part of the Gulf of Alaska (NGOA) has been the focus of several scientific projects (e.g. Fisheries Oceanography Coordinated Investigations–National Oceanographic and Atmospheric Administration, Gulf Apex Predator–prey study—University of Alaska Fairbanks) interested in understanding the causes of decline of Steller sea lion (*Eumetopias jubatus*) populations (Loughlin & York, 2000; Wynne & Foy, 2002). Nutritional stress caused by climate variability is one of the most important factors explaining such decline first detected 30-years ago (Trites & Donnelly, 2003;

Trites et al., in press). Since prey availability for Steller sea lions is linked to phytoplankton biomass (*B*) distributions (Hirons et al., 2001), monitoring of *B* represents a fundamental tool to figure out changes in sea lions dynamics under different environmental conditions. Multiple factors affect the spatial distribution of *B* over the NGOA shelf and change during the year (e.g. nutrient availability, zooplankton grazing) (Brickley & Thomas, 2004; Stabeno et al., 2004).

In NGOA waters, global spatial patterns of chlorophyll *a* concentration (*chl*), a *B* proxy, have been studied using standard satellite algorithms (Brickley & Thomas, 2004). However, satellite footprint limits small-scale detection (<1 km) of *chl* variations. Likewise, stray light from land (Reinersman & Carder, 1995) and bottom radiance contribution in shallow waters (<30 m) (Lee et al., 2001) contaminate near shore pixels.

\* Corresponding author. Tel.: +1 727 553 3952; fax: +1 727 5533918.

E-mail address: [mmontes@mail.usf.edu](mailto:mmontes@mail.usf.edu) (M.A. Montes-Hugo).

Synoptic chl mapping using ship surveys has not been feasible in shelf waters of NGOA due to the dynamic conditions (e.g. strong winds, long-shore transport) (Stabeno

et al., 2004) and restricted access to shallow areas (Brown et al., 2002). The use of airborne remote-sensing (Lee et al., 2001; Brown et al., 2002) provides a possible solution to estimate

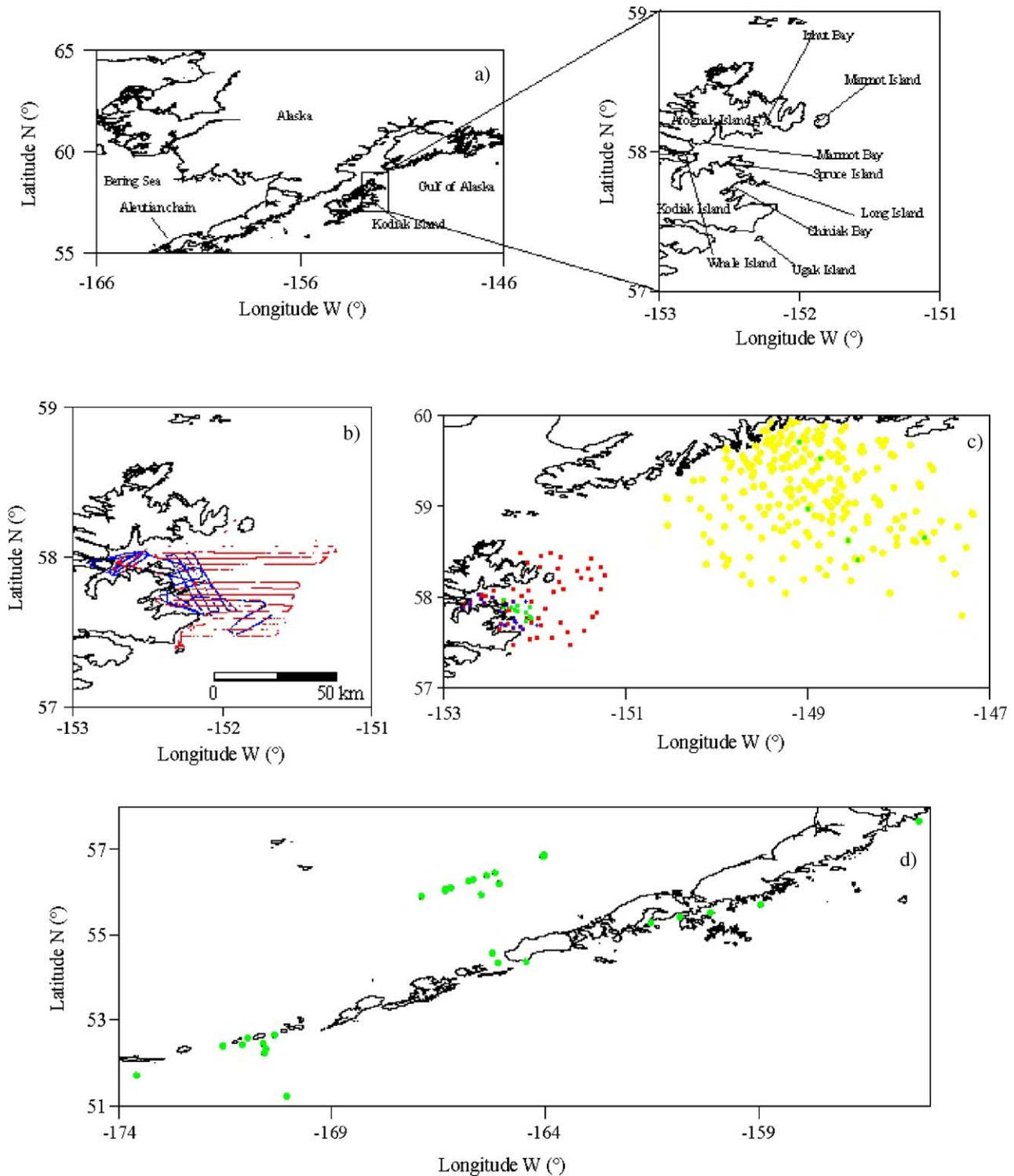


Fig. 1. Airborne, ship and satellite surveys over the study area. (a) Geographic location of Afognak/Kodiak Islands in the northern part of the Gulf of Alaska; the small inset showed with more detail the area where pigment concentrations were estimated during aerial measurements, (b) flight tracks during July (red dots) and August (blue dots) 2002, (c) field chl measurements of FOY dataset (2002 July: red dots, August: blue dots), PEGAU dataset (2003, May–July–August) image coordinates (yellow dots); Validation points of airborne  $R_{rs}$ –chl relationship (green dots) based on shipboard, satellite (SeaWiFS) and airborne reflectance measurements; notice that all chl sampling stations of CARDER dataset in Bering Sea (d) were used to test the chl remote-sensing models (For interpretation of the references to colour in this figure legend, the reader is referred to the web version of this article.).

small-scale horizontal distributions ( $\sim 0.1$  km) of chlorophyll values under fluctuating conditions such as the NGOA. Aerial surveys allow synoptic views, are faster and less expensive than ship cruises (Brown et al., 2002), and unlike satellites, flights can be scheduled at various times per day to accommodate tidal and meteorological conditions. Also, the path-radiance (aerosols+air molecules) observed in imagery from low-flying airplanes ( $\sim 0.3$  km above sea surface) is minor compared to that observed from satellite platforms relative to the water-leaving signal. Atmospheric correction of satellite imagery in high-latitudes environments such NGOA is not straightforward because the larger sun angles with respect to zenith. At zenith angles above  $50^\circ$ , single-scattering approximation for Rayleigh contribution fails, and multiple-scattering algorithms must be used instead (Gordon et al., 1988).

The aim of the present study was to estimate horizontal distributions of chl values in coastal waters of NGOA using high-resolution airborne data. Regarding the economic and ecological interest of Steller sea lion–fish interactions, the final intention is to localize areas in the NGOA with relative high productivity and their relationships with environmental variables, and oceanographic features (e.g. fronts). Airborne spectral upwelling radiances and downwelling PAR (photo-synthetically available radiation) irradiance (400–700 nm) data were gathered over waters of the eastern shelf of Afgonak/Kodiak Islands during summer (July–August) of 2002 (Fig. 1a). These shelves are highly influenced by southern branch of the Alaska Coastal Current, and had been historically more productive than other NGOA regions, even during summer conditions when a strong thermocline is present (Stabeno et al., 2004). Performance of band-ratio and spectral curvature remote-sensing reflectance ( $R_{rs}$ ) algorithms to retrieve chl values were evaluated with simultaneous measurements of chl and  $R_{rs}$  data. Field surveys of ancillary variables (e.g. temperature, water transparency) were coordinated with aerial missions.

## 2. Methods

### 2.1. Atmospheric correction

Remote-sensing measurements from airplanes usually do not require extensive atmospheric path-radiance corrections unless airborne spectra are obtained from relative high altitudes (e.g.  $>3$  km for Airborne visible Infrared Imaging Spectrometer). In this work, downwelling irradiance above sea-surface values ( $E_d^+$ ) were interpolated for each flight in order to find cloud-free areas potentially suitable for total radiance above-water measurements ( $L_t(\lambda)$ ). A quasi-single-scattering approximation was suggested (Rayleigh–aerosol multiple scattering ignored) to relate water-leaving radiance ( $L_w$ ) to  $L_t$  (Gordon et al., 1983):

$$L_t(\lambda) = L_r(\lambda) + L_a(\lambda) + t(\lambda)L_w(\lambda) \quad (1)$$

where  $t(\lambda)$  is diffuse transmittance of the atmosphere, and  $L_r$  and  $L_a$  are Rayleigh and aerosol radiances. Values of  $L_r$  are

computed as follows:

$$L_r(\lambda) = [\omega_r(\lambda)\tau_r(\lambda)F'_0(\lambda)p_r(\theta, \theta_o, \lambda)]/4\pi \quad (2)$$

$$p_r(\theta, \theta_o, \lambda) = \{P_r(\theta_-, \lambda) + [\rho(\theta) + \rho(\theta_o)]P_r(\theta_+, \lambda)\}/\cos\theta \quad (3)$$

$$P_r(\theta_{\pm}, \lambda) = 3/4[1 + \cos^2\theta_{\pm}] \quad (4)$$

$$\cos\theta_{\pm} = \pm\cos\theta_o\cos\theta + \sin\theta_o\sin\theta\cos(\phi - \phi_o) \quad (5)$$

where  $\omega_r$  is the single-scattering albedo of water molecules,  $\theta_o$  and  $\phi_o$  are the solar zenith and azimuth angles,  $\theta$  and  $\phi$  are the zenith and azimuth angles of a vector from the point of the sea-surface to the sensor,  $P_r$  is the Rayleigh phase function, and  $\rho(\theta)$  is the Fresnel reflectance. Skylight reflectance effects were accounted with a first-order adjustment by subtracting  $L_{780}$  to  $L_t(\lambda)$  in Eq. (1) (Lee et al., 2001). Rayleigh optical thickness ( $\tau_r$ ) interpolated between 0 and 1 km was provided by Eltermann (1968) tables. Since the aircraft was flying well below the ozone layer,  $t(\lambda)$  was calculated considering an aerosol transmittance equal to 1 (Gordon & Clark, 1980). Path-radiance due to aerosol scattering was calculated over clear-water pixels where a minimum water-leaving radiance at 665 nm is expected ( $L_a^o = L_t(665) - L_r(665)$ ). Contribution of aerosol scattering to  $L_t(\lambda)$  was then estimated:

$$L_a(\lambda) = S(\lambda_i, \lambda_o)L_a^o \quad (6)$$

$$S(\lambda_i, \lambda_{665}) = \varepsilon(\lambda)F'_0(\lambda)/F'_0(665) \quad (7)$$

where  $\lambda_i = 411, 443, 491, 509, 553$ , and  $\lambda_o = 665$  nm.

A value of  $\varepsilon(\lambda) = 1$  was assumed in this study as a first-order correction applicable to maritime atmospheres as in standard Coastal Zone Color Scanner (CZCS) processing (Gordon et al., 1983).  $F'_0(\lambda)$  is equal to the instantaneous extraterrestrial solar irradiance  $F_o(\lambda)$  (ozone optical thickness=0). Values of  $F_o(\lambda)$  were obtained from Neckel and Labs (1984) tables. Measurements of  $L_t(\lambda)$  and  $E_d^+(\lambda)$  were performed at 411, 443, 491, 509, 553, 665, and 780 nm (10 nm bandwidth) with a Micro Surface Acquisition System (MicroSAS). The spectrometric system has two digital optical sensors ( $L_t(\lambda)$ : OCR-507-R03A,  $E_d^+(\lambda)$ : OCR-507-ICSA, Satlantic inc., Canada). As specified by the manufacturer, field-of-view of the radiance sensor is  $28^\circ$  in air, and has a typical saturation of  $5 \mu\text{W cm}^{-2} \text{nm}^{-1}$ . The irradiance sensor has a typical saturation of  $300 \mu\text{W cm}^{-2} \text{nm}^{-1}$  and a noise equivalent input of  $2.5 \times 10^{-3} \mu\text{W cm}^{-2} \text{nm}^{-1}$ .

Aerosol horizontal distribution over the aerial transects was estimated from values of aerosol optical thickness at 865 nm ( $\tau_{865}$ ) obtained from Sea-viewing Wide Field-of-view Sensor (SeaWiFS) images during the period studied.

### 2.2. Empirical airborne methods for deriving chl from remote-sensing measurements

Similar to satellite-borne sensors, development of airborne empirical chl models is still on-going (Harding et al., 1994; Sathyendranath et al., 2004). Airborne color algorithms remain

basically comparable to those of satellite remote-sensing relationships since both types of remote-sensing platforms have been sharing almost the same spectral resolution, and in some cases even the same color channels (e.g. Daedalus spectrometer matches CZCS).

Empirical satellite chl algorithms are based on nadir-normalized water-leaving radiance ( $nL_w$ ) and remote-sensing reflectance ( $R_{rs}(\lambda) = L_w(\lambda)/E_d^+(\lambda)$ ) ratios (O'Reilly et al., 1998). Spectral-curvature or inflection-ratio chl algorithms have been used without atmospheric correction at low aircraft altitudes since the 80's (e.g. Campbell & Esaias, 1983). These models are very sensitive to curvature changes ( $G$ ) of  $R_{rs}$  around a centered wavelength  $\lambda_i$  (e.g. 490 nm):

$$G_{m,n}(\lambda_i) = s(\lambda_i)^2 / (s(\lambda_i - m)s(\lambda_i + n)) \quad (8)$$

where  $s$  is the remotely sensed water property (e.g.  $R_{rs}$ ) and  $n$ ,  $m$  vary between 1 and 2.

Although  $G$  and band-ratio algorithms may cover a wide range of field chl (0.1–10 mg m<sup>-3</sup>) values (Campbell & Esaias, 1983; Gordon & Morel, 1983), these remote-sensing chl estimates (chl<sub>FOD</sub>) can only be retrieved from the first optical depth ( $z=1/\text{beam attenuation coefficient}$ ) due to the exponential signal decrease with depth (Gordon & McCluney, 1975). Moreover, performance of these empirical algorithms may be deteriorated in Case II waters (i.e. those waters where inherent optical properties are also dominated by constituents such gelbstoff) (Campbell & Esaias, 1983; Sathyendranath et al., 2004). In this work, performance of four modified cubic-polynomial band-ratio (OC2a =  $R_{rs}(412)/R_{rs}(553)$ , OC2b =  $R_{rs}(443)/R_{rs}(553)$ , OC2 =  $R_{rs}(491)/R_{rs}(553)$ , OC2d =  $R_{rs}(509)/R_{rs}(553)$ ) (O'Reilly et al., 1998), and one Grew-type spectral-curvature ( $G_{1,1}(491) = R_{rs}(491)^2 / (R_{rs}(443)R_{rs}(509))$ ) model (Campbell & Esaias, 1983) were tested to estimate chl<sub>FOD</sub> values in NGOA waters. According to the literature, selected chl algorithms were the most reliable as global indicators of chl (Grew, 1980; O'Reilly et al., 1998).

### 2.3. Field measurements

The ultimate goal of this work is to use airborne chl remote-sensing algorithms to identify productive areas and their relation with environmental conditions in the NGOA. Thus, description of ancillary field information (meteorology and hydrography) during aerial missions was essential to interpret horizontal chl variations and evaluate whether chl remote-sensing estimates were meaningful from the oceanographic point of view.

Aerial surveys of  $L_t(\lambda)$  and  $E_d(\lambda)$  were effectuated during 27–28 July, and 17 August 2002 on the eastern shelves of the Afgonak/Kodiak Islands (Fig. 1b). Airborne sampling lines were designated to cover a number of different water masses/features including shallow banks (~50 m), troughs (up to 200 m) and areas with small islands. Surveys during July were complementary while August transects overlapped July ones circa 58° N to the south. More intense flight measurements were carried out in Marmot Bay around Whale Island due to

the relatively elevated productivity of these waters (Dr. Robert Foy, pers. comm.). As suggested by Campbell and Esaias (1983), flight times were scheduled according to the sun's elevations between 20° and 50° to avoid sun glint.

At 300 m altitude (average height during flights), across track data collections had a maximum spatial resolution of 72.5 m. This corresponded also with the minimum pixel size since the radiance detector was positioned with a zero zenith angle. Although the MicroSAS sampling rate was 6 data (7 channels) per second and every 65 m (along track distance), original radiometric readings were binned every 200 m (~3 s) by averaging. Geo-located radiance and irradiance data were corrected for pitch, roll and height for each flight.

Preliminary results showed that chl field measurements matching  $R_{rs}$  data during aerial surveys were insufficient, thus shipboard and satellite  $R_{rs}$  data were additionally analyzed. Field surveys for testing chl remote-sensing algorithms were carried out during 14–16, 19–29 July, 16–18 August 2002 (FOY dataset), and 1–21 May, 21 July–12 August 2003 (PEGAU dataset) (Fig. 1c). FOY and PEGAU chlorophyll concentrations were matched with cloud-free satellite reflectance spectra (SeaWiFS) within three hours of the satellite pass. Likewise, only scenes between 9:00 and 15:00 h (local time) were collected. L2 imagery products ( $R_{rs}$  at 412, 443, 490, 510, and 555 nm) were obtained from DAAC (<http://daac.gsfc.nasa.gov>) and processed using 5-by-5 pixel means with SEADAS 4.6 software. Further validation of selected chl remote-sensing algorithm was effectuated with in situ  $R_{rs}$  and chl data obtained in Bering Sea during 18–19, 21–28 April 1996 (CARDER dataset).

Briefly, in situ upwelling radiance and sky radiance spectra were measured 90° from the solar plane and 30° from nadir and zenith, respectively (Lee et al., 1996). Additional radiance measurements were made perpendicular to a graycard reflector ( $L_G(\lambda)$ ) with a known reflectance ( $R_G(\lambda)$ ) for each suite of  $R_{rs}$  values. All measurements for the CARDER dataset were performed using an above-water hand-held spectroradiometer (~350–850 nm; 512-channel, 10° field-of-view) (Lee et al., 1996). Values of  $E_d^+$  were computed:

$$E_d^+ = \pi L_G / R_G \quad (9)$$

Calculating the water-leaving radiance is more difficult since measurements of  $L_t$  must be corrected for reflected sky radiance ( $L_{sky}$ ) and possible solar glint. Water-leaving radiance spectra were calculated as:

$$L_w = L_t - (\rho(\theta)L_{sky} + \Delta) \quad (10)$$

where  $\Delta$  is a solar glint correction derived assuming  $R_{rs}(750)$  equal to zero.

Scans with anomalously high  $L_t(750)$  values were omitted to minimize glint effects. Multiple measurements were taken of  $L_t$ ,  $L_G$ , and  $L_{sky}$ .

Only for FOY stations, vertical profiles of chl, PAR, temperature, and salinity were made. Sampling lasted from 10:00 to 15:00 h daily, and had an average working period per station of 30 min. For each  $R_{rs}$ -chl comparison, every chl<sub>FOD</sub>

was the average of chl samples between zero and the first attenuation depth ( $\sim 7$  m,  $\sim 90\%$  of  $L_w$  is originated at that depth) (Gordon & McCluney, 1975). Pigment concentration was determined by fluorescence after extraction with acetone 90% (Venrick & Hayward, 1984). Surface and underwater downward PAR were determined with a light-meter LI-COR (LI-190SB, LI-192SB) (precision:  $\pm 5\%$  as quoted by the manufacturer — LiCor Inc., Lincoln, Nebraska). PAR transmission was calculated within the upper mixed layer as the ratio between PAR values measured at 20 and 0 m ( $T_{20}$ ). Integrated chl within the euphotic zone ( $B_{EU}$ ) was obtained by trapezoidal integration between zero and the euphotic depth ( $z$  at which PAR equal 1% of surface PAR). Daily L3 coastal wind data (25 km resolution, SeaWinds sensor, <http://podaac.jpl.nasa.gov>) were used to interpret aerosol origins, and modeled chl distributions.

In coastal waters influenced by freshwater inputs, gelbstoff is inversely related to salinity (Blough et al., 1993). Hence, the potential effect of gelbstoff on airborne chl estimates was assessed using surface salinity fields during each flight track. Likewise, a numerical filter originally proposed for satellite data was applied to airborne  $R_{rs}(\lambda)$  ratios to identify gelbstoff-rich waters over the study area (Carder et al., 1999):

$$R_{rs}(412)/R_{rs}(443) = 0.95[R_{rs}(443)/R_{rs}(553)]^{0.16} \quad (11)$$

Original MODIS wavelengths are slightly different from MicroSAS wavelengths (e.g. 551 nm instead of 553 nm) even though these differences ( $\sim 2$  nm) may be considered negligible (O'Reilly et al., 1998). Airborne  $R_{rs}(\lambda)$  ratios falling below the case I water (i.e. phytoplankton and its metabolic products dominate water optical properties) relationship (11) indicate high-gelbstoff data points. Notice that filter (11) also provides a space-based method to separate data points with packaged pigments (points below case I curve) from those with unpackaged pigments. Pigment-package effect is manifested as a flattening on phytoplankton absorption peaks with increasing intracellular pigment concentration due to shelf-shading (Morel & Bricaud, 1981).

To quantify the influence of bottom depth on  $nL_w$  and  $R_{rs}$  spectra measurements and describe ecologic effects of hydrographic features on chl distributions, high-resolution bathymetry ( $\sim 8.3$  km) around Afgonak/Kodiak Islands (Pacific Marine Environmental Laboratory, Hermann et al., 2002) was analyzed. High-resolution coastline ( $\sim 0.2$  km) was obtained by plotting closed polygons of Global Self-consistent hierarchical shoreline database (Wessel & Smith, 1996). Water depth in Afgonak/Kodiak shelves is very influenced by tidal variations (up to 2.5 m amplitude). Water level data relative to the mean

low level water (MLLW) was obtained from Kodiak tidal prediction station in Kodiak Island (NOAA/NOS, <http://co-ops.nos.noaa.gov>).

Changes on  $nL_w$  and  $R_{rs}$  spectra due to different water column stabilities during summer are also expected in NGOA waters. Thus, water column mixing was estimated based on vertical density differences measured between surface and pycnocline depth ( $d\rho$ ).

#### 2.4. Statistical analysis

Band-ratio and spectral-curvature relationships were log-transformed, and their performance to estimate  $chl_{FOD}$  was compared using the root mean square error in  $\log_{10}$  scale of quantity between  $N$  derived and true values (O'Reilly et al., 1998):

$$RMSE_{\log_{10}} = \left\{ \sum [\log_{10}(chl_{FOD}^{derived}) - \log_{10}(chl_{FOD}^{true})]^2 / N \right\}^{0.5} \quad (12)$$

The difference between derived and true  $chl_{FOD}$  values in linear scale is computed as:

$$\epsilon_{tr} = 0.5 * [(10^{RMSE_{\log_{10}}} - 1) + (1 - 10^{-RMSE_{\log_{10}}})] \quad (13)$$

To estimate the proportion of variation explained by  $chl_{FOD}$  remote-sensing models, calculation of coefficient of determination ( $R^2$ ) was carried out using minimization routines (IDL, Research System incorporated). Likewise, goodness of fitting of spectral-curvature models was evaluated using linear regression of  $\log$ – $\log$   $R_{rs}$ – $chl_{FOD}$  data as suggested by Campbell & Esaias (1983). Time series of estimated  $chl_{FOD}$  horizontal fields was obtained by kriging interpolation using contouring and surface mapping commercial software.

### 3. Results

#### 3.1. Airborne water-leaving radiance and reflectance

Ambient light parameters, position and bottom depths encompassed during 2002 MicroSAS surveys are summarized in Table 1. North–central (27 July), southern (28 July), and south–central (17 August) aerial surveys covered a total of  $5.34 \cdot 10^3$  km<sup>2</sup> (3800 stations). Mean of water-leaving radiance at 665 nm in clear waters ( $57.84^\circ$  N,  $-150^\circ$  W) and for the whole period surveyed was  $0.078 \pm 0.0005 \mu W \text{ cm}^{-2} \text{ nm}^{-1} \text{ sr}^{-1}$  ( $L_t(665) = 0.131 \mu W \text{ cm}^{-2} \text{ nm}^{-1} \text{ sr}^{-1}$ ,  $L_r(665) = 0.0543 (\mu W \text{ cm}^{-2} \text{ nm}^{-1} \text{ sr}^{-1})$ ). Values of  $\tau_{865}$  were fairly constant

Table 1  
Flight track ancillary data and main remote-sensing variables during aerial surveys over coastal waters of Afgonak/Kodiak shelves

Date	Time	Acov	Lat	Lon	Zcov	$\theta_o$	$D$
7/27/02	7:00–12:55	3.68	57.71, 58.71	–152.75, –151.08	21–260	39.8–51.3	16.5
7/28/02	9:00–10:33	1.18	57.39, 57.73	–152.46, –151.54	11–221	41.9–50.8	16.3
8/17/02	9:00–11:20	1.66	57.48, 58.04	–152.91, –151.67	50–216	45.6–55.5	15.0

Time: local time, Acov: surface area coverage (km<sup>2</sup>)  $10^3$ , Lat: latitude ( $^\circ$ ), Lon: longitude ( $^\circ$ ), Zcov: bottom depth range (m),  $\theta_o$ : solar zenith angle ( $^\circ$ ),  $D$ : photoperiod (h).

throughout the airborne surveys ( $0.072 \pm 0.006$ ). Wind direction data from SeaWinds indicated most of the time a predominant maritime origin of aerosols. Airborne  $nL_w(\lambda)$  and  $R_{rs}(\lambda)$  measurements are summarized in Table 2.

Water-leaving radiance and remote-sensing reflectance were perhaps influenced by hydrodynamics affected by the intricate bathymetry of Afgonak/Kodiak shelves (Fig. 2). Apparently, some  $nL_w$  and  $R_{rs}$  spectra presented a maximum at 553 nm such as those observed in very shallow waters (<30 m) (Fig. 2a). However, the reflectance valley formed between channel 3 and 5 may be attributed to a Fraunhofer absorption line centered at 519 nm, and mismatch of spectral calibration of MicroSAS filters. Highest (e.g. Stations A–C) values of  $R_{rs}$  were generally observed near the coast close to small islands (Fig. 2b). Along these areas, high load of sediments and detritus is expected, consistent with a fresher water supply near the coast. Notice in Fig. 2a that the steepest slope between 411 and 491 nm (station F) was likely related to higher concentration of gelbstoff and chl. With the exception of 665 nm channel, values of  $nL_w$  and  $R_{rs}$  values decreased for all MicroSAS channels from 27 July to 28 July, and increased again on 17 August (Table 2).

### 3.2. Chlorophyll models

The log-transformed ratio  $R_{rs}(509)/R_{rs}(553)$  (OC2d) was most consistent with log-transformed field  $chl_{FOD}$  data ( $chl_{FOD}$  range between 0.2 and 11  $mg\ m^{-3}$ ) from FOY 2002 and PEGAU 2003 datasets as shown on Figs. 3 and 4, and Table 3. In Fig. 3, only SeaWiFS  $R_{rs}$  data vs. field chl measurements are plotted. The bio-optical relationships in log–log scale clearly illustrate the poorer performance of blue-based ratios (69% of residual explained) (Table 3) to derive chl values in our study area. In general for all chl band-ratio tested, there were not marked differences between field and modelled  $R_{rs}$  data for stations with low (<0.3  $mg\ m^{-3}$ ) and high (>1.5  $mg\ m^{-3}$ ) chl values (Fig. 3a–c). In Fig. 3d, functionalities between a spectral-curvature algorithm ( $G_{1,1}(491)$ ) and  $chl_{FOD}$  is explored by fitting a linear regression curve. Regression analysis of  $chl_{FOD}-G_{1,1}(491)$  relationship was not significant at the 95% confidence level, and confirmed the weakness of using relative short wavelengths to retrieve pigments in coastal environments of Alaska.

In Fig. 4, additional in situ shipboard and airborne calibrated  $R_{rs}$  values are presented to verify the tighter relationship between  $R_{rs}(509)/R_{rs}(553)$  and  $chl_{FOD}$  measurements observed

with SeaWiFS imagery. Notice that Fig. 4a contains data for different years and obtained with diverse sensors (e.g. shipboard, airborne vs. spaceborne) and atmospheric corrections schemes. Regardless of the dataset used, most of the chl points computed with OC2d were underestimated compared to in situ pigment concentrations because modelled chl values were located below the 1:1  $chl_{FOD}$  line (Fig. 4b). For the whole pool of  $chl_{FOD}-R_{rs}(509)/R_{rs}(553)$  pairs ( $n=56$ ),  $R^2=0.84$ ,  $RMSE_{\log_{10}}=0.20$ , linearized  $\epsilon_{tr}=0.48$ . Part of the residual variability between estimated and  $chl_{FOD}$  measurements in Fig. 4b were connected with local changes in water optical properties. For instance, some stations of CARDER dataset were performed in coastal waters of Bering Sea where high load of sediments due to riverine influence (e.g. Yukon River) is expected. Moreover, airborne  $R_{rs}$  data evidenced a bias with respect to the 1:1  $chl_{FOD}$  line that can be accounted for an incomplete removal of atmospheric contribution from radiance values above the water.

### 3.3. Spatial distribution of estimated chlorophyll

The band-ratio OC2d algorithm provided retrieval most consistent with  $chl_{FOD}$  measurements in our study. However, relatively high variability of estimated  $chl_{FOD}$  values using OC2d compromised calculation of absolute pigment concentrations with our dataset. Thus, OC2d relationship was used instead to obtain an index of  $chl_{FOD}$  during each flight mission and for different areas of Afgonak/Kodiak shelves.

The mean of  $chl_{FOD}$  calculated from  $R_{rs}(509)/R_{rs}(553)$  values ( $chl_{FODest}$ ) was 3.45 (standard error=se=0.05,  $n=1794$ ), 2.68 (se=0.08,  $n=879$ ), 4.44 (se=0.09,  $n=1928$ ) for 27, 28 July and 17 August 2002, respectively. On 27 July, high pigment patches (7–10  $mg\ m^{-3}$ ) developed preferentially over the central part of N. Albatross Bank, and along a zone between Spruce and Whale Island (Figs. 2b and 5a). On 28 July, relatively high  $chl_{FODest}$  values ( $\sim 10\ mg\ m^{-3}$ ) were again found over N. Albatross Bank and along nearshore areas of Ugak Island and Chiniak Bay mouth (Fig. 5b). On 17 August,  $chl_{FODest}$  values above 7  $mg\ m^{-3}$  were widespread and distributed from the entrance of Marmot Bay to the entrance of Chiniak Bay (Fig. 5c). Similar to 28 July, rich chl waters were also present near Ugak Island and eastward of Chiniak Bay entrance over N. Albatross Bank. Notoriously,  $chl_{FODest}$  values up to 20  $mg\ m^{-3}$  were principally calculated east of Long Island (Fig. 5c).

Table 2  
Water-leaving radiance and remote-sensing reflectance measurements over coastal waters of Afgonak/Kodiak shelves

Date	$nL_w$						$R_{rs}^a$					
	411	443	491	509	553	665	411	443	491	509	553	665
7/27/02	0.326 (0.005)	0.406 (0.006)	0.478 (0.007)	0.448 (0.006)	0.443 (0.006)	0.364 (0.017)	3.9	4.4	4.7	4.5	4.6	3.8
7/28/02	0.166 (0.003)	0.219 (0.004)	0.272 (0.004)	0.242 (0.004)	0.219 (0.004)	0.172 (0.012)	2.2	2.6	2.9	2.6	2.6	1.9
8/17/02	0.228 (0.008)	0.275 (0.010)	0.319 (0.013)	0.279 (0.013)	0.329 (0.020)	0.154 (0.015)	2.7	3.0	3.0	2.6	3.3	1.0

$nL_w$ : nadir-normalized water-leaving radiance ( $\mu W\ cm^{-2}\ nm^{-1}\ sr^{-1}$ ),  $R_{rs}$ : remote-sensing reflectance ( $sr^{-1}$ ) ( $10^{-3}$ ). MicroSAS channels (nm) are indicated in the second row. Between parentheses is one standard error.

<sup>a</sup> Standard error for all wavelengths was  $1 \times 10^{-4}$ .

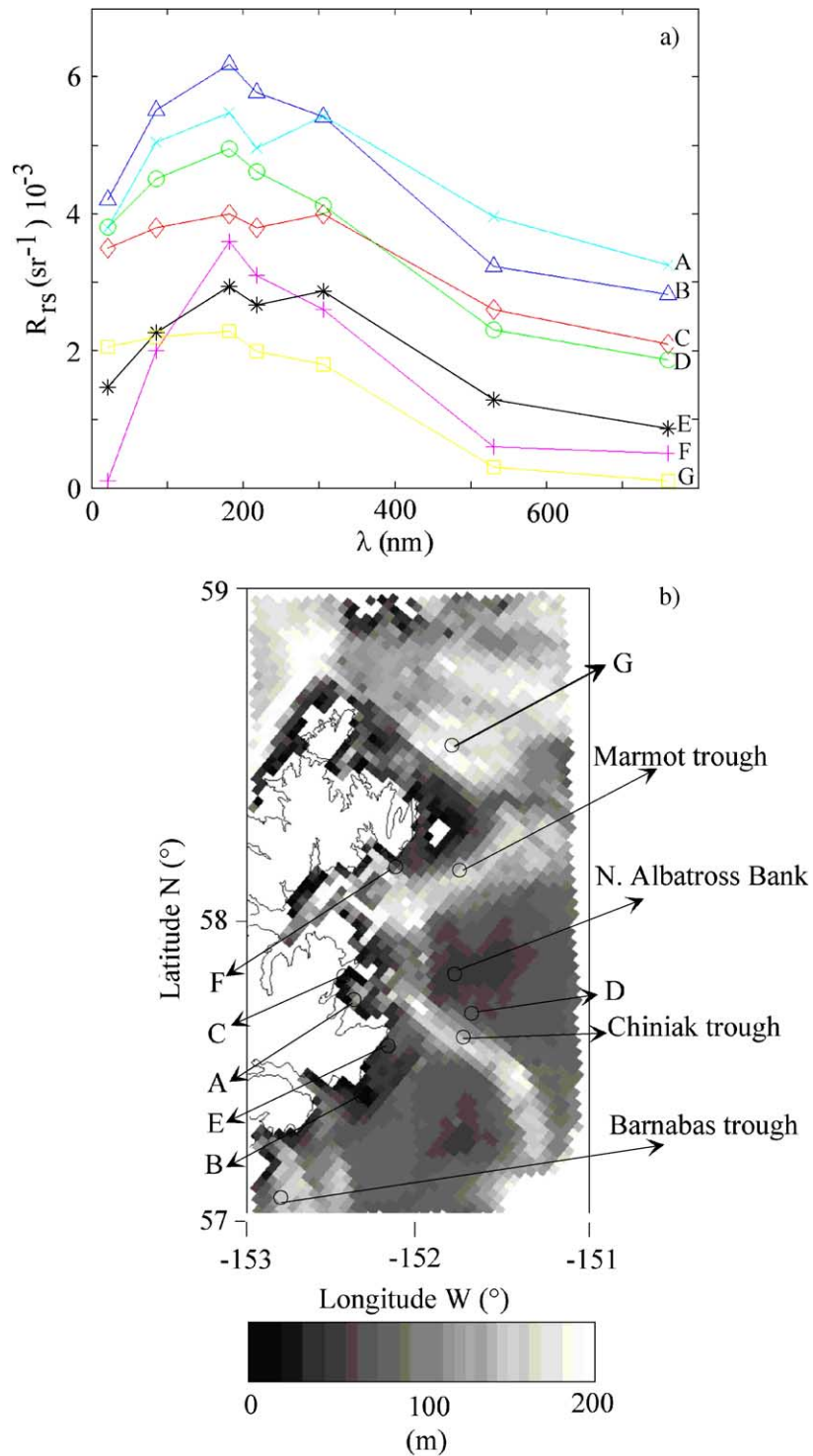


Fig. 2. Typical remote-sensing reflectance spectra and bathymetry of Afognak/Kodiak shelf waters. (a) Spectral reflectance curves for shallow/deep and inshore/offshore waters, (b) Bathymetric levels on the eastern shelf of Afognak/Kodiak Islands and position of  $R_{rs}(\lambda)$  spectra, Fig. 2a. Shallow banks (<50 m) and troughs (~200 m) are represented with black and white colors, respectively. Portlock bank is situated northeast of Marmot Island ( $58.5^{\circ}$  N,  $-150.5^{\circ}$  W).

In terms of regional trends,  $\text{chl}_{\text{FODest}}$  provided the highest values in the southeastern stations of the time series over the N. Albatross Bank (Fig. 5). This area was characterized by warm waters ( $\sim 10^{\circ}\text{C}$ ) and a weakly water column stratification ( $\delta\rho=0.4$ ) (Fig. 6a,c). Chlorophyll enrichment of banks is expected based on previous field observations made in Portlock

Bank (northeast of Marmot Bay) by Kachel et al. (2003). Introduction of nutrients into the euphotic zone due to topographic steering was a potential mechanism explaining these elevated pigment concentrations (Kachel et al., 2003). Low PAR transmission at 20 m depth ( $\sim 5\%$ ) did not suggest a spatial connection between underwater PAR levels and high chl

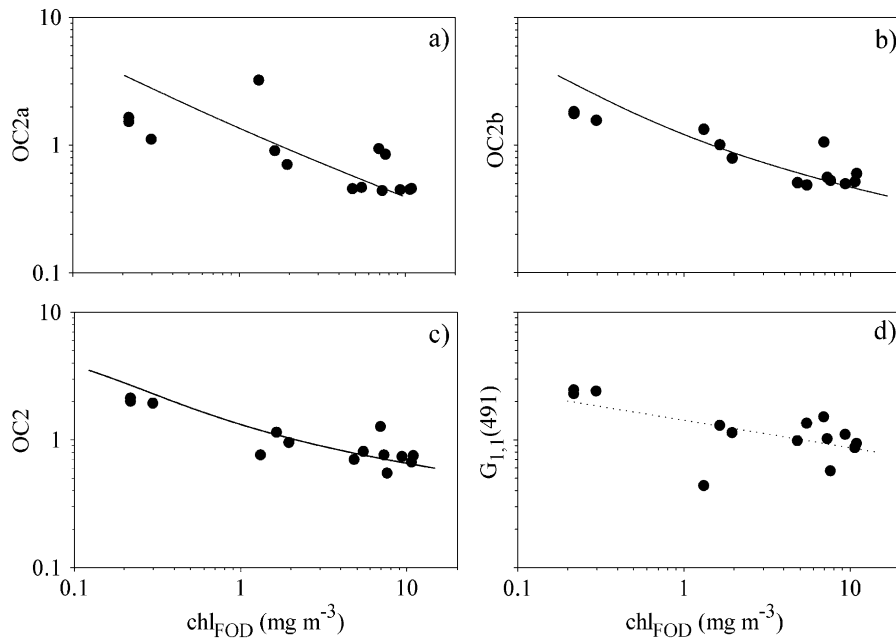


Fig. 3. Performance of band-ratio and spectral-curvature algorithms to retrieve chlorophyll *a* concentrations from the first-optical depth ( $\text{chl}_{\text{FOD}}$ ) of Alaskan Coastal waters. (a–c) SeaWiFS band-ratio models, (d) Grew-type spectral-curvature model; modified cubic polynomial models of chl (solid line) (O'Reilly et al., 1998), linear regression fitting (dotted line), FOY and PEGAU field data (solid circles).

values found over N. Albatross Bank (Fig. 7a). High chl patches (up to  $12 \text{ mg m}^{-3}$ ) were also observed at the entrance of Marmot Bay and Chiniak Bay, and coincided with relative low water temperatures ( $\sim 9^\circ \text{C}$ ), homogeneous vertical density profiles, and large bathymetric changes ( $> 150 \text{ m}$  in less  $10 \text{ km}$  across the entrance) (Figs. 2 and 6a,c). Although these areas cannot be discarded as high primary productivity spots (see Discussion), high chl values within the first optical depth could also be attributed to vertical redistribution of phytoplankton cells. In general, a prominent sub-surface B peak was characteristic during the period studied except in those areas with relatively high vertical mixing.

Spatial variability of estimated  $\text{chl}_{\text{FOD}}$  values was consistent with field integrated chl values throughout the euphotic zone during July–August 2002. Indeed, highest  $B_{\text{EU}}$  measurements were found over N. Albatross bank ( $> 500 \text{ mg m}^{-2}$ ), and along the entrance of Marmot Bay and Chiniak Bay ( $\sim 400 \text{ mg m}^{-2}$ ) (Figs. 5 and 7b). Likewise, minimum OC2d retrievals matched low  $B_{\text{EU}}$  waters ( $\sim 150 \text{ mg m}^{-2}$ ) such as in the innermost part of Bays, and Marmot trough. A reduced vertical transport of bottom nutrients is expected in these areas due to a well defined pycnocline ( $\delta\rho = 0.8$ ) driven by land freshwater inputs ( $S < 30$  to the head of Marmot Bay) (Figs. 5, 6b,c and 7b) (see Discussion).

The mean of  $\text{chl}_{\text{FODest}}$  for the scene was significantly higher during 17 August than that calculated for 27–28 July ( $3.20 \pm 0.04$ ). This rise on estimated pigment levels during August surveys also corresponded with higher water temperatures (July:  $10.93 \pm 0.32^\circ \text{C}$ , August:  $9.31 \pm 0.18^\circ \text{C}$ ), higher water column stratification ( $\rho = 0.31 \pm 0.04$ ,  $\rho = 0.22 \pm 0.03$ ), higher surface light levels ( $E_d^+(780)$  July:  $38.3 \pm 0.4 \mu\text{W cm}^{-2} \text{ nm}^{-1}$ , August:  $68.3 \pm 0.2 \mu\text{W cm}^{-2} \text{ nm}^{-1}$ ), lower wind speeds (July:  $4.5 \text{ m s}^{-1}$ , August:  $3.5 \text{ m s}^{-1}$ ), and lower

salinities (July:  $31.90 \pm 0.08$ , August:  $31.55 \pm 0.16$ ). Summarizing, these environmental conditions were favorable for phytoplankton growth because the greater light availability, water temperature, and shallower mixed layer (see Discussion).

Higher  $\text{chl}_{\text{FODest}}$  values and light levels in August with respect to July were not related with relative poor-gelbstoff waters during August. Percentage of points with 'high-gelbstoff/high-package effect' flagging was higher in July ( $\sim 60\%$ ) than in August ( $\sim 41\%$ ) (Fig. 8). However, higher salinities in July and comparable July–August PAR transmissions ( $T_{20} \sim 6.2\%$ ) suggested a major influence of phytoplankton photoacclimation on gelbstoff numerical filter (Eq. (11)) (Figs. 6b, 7a and 8).

#### 4. Discussion

In this study, high-resolution airborne  $R_{\text{rs}}$  data was used to estimate chl patchiness over coastal waters of Afognak/Kodiak Islands during summer of 2002. Changes in phytoplankton biomass have been hypothesized to affect the prey availability for Steller sea lion populations of NGOA (Trites et al., in press). The measurement of ancillary data (temperature, salinity, PAR) during  $R_{\text{rs}}$  aerial surveys was an indispensable tool to elucidate why hot spots of chl estimated with  $R_{\text{rs}}$  relationships have a preferential location or timing in Afognak/Kodiak shelves.

The ratio  $R_{\text{rs}}(509)/R_{\text{rs}}(553)$  was the best index of  $B$  levels in surface waters of NGOA waters. The success of OC2d in our study may be related to the importance of phytoplankton light scattering over absorption when chl is relatively high ( $> 5 \text{ mg m}^{-3}$ ) (Campbell & Esaias, 1983). O'Reilly et al. (1998) found that band-ratio  $R_{\text{rs}}(510)/R_{\text{rs}}(555)$  yields the lowest RMS when chl values are well above  $1.5 \text{ mg m}^{-3}$ . O'Reilly et al. (1998)

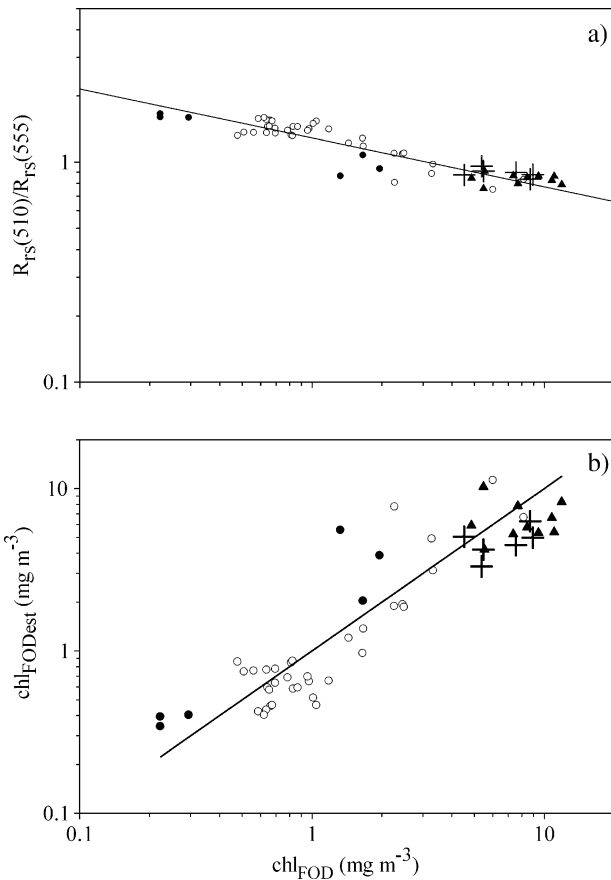


Fig. 4. Airborne remote-sensing algorithms to estimate chlorophyll in coastal waters of NGOA. (a) log–log relationship between reflectance ratio and chl measurements for the first optical depth, theoretical chl values calculated from OC2d algorithm and using  $R_{rs}(510)/R_{rs}(555)$  values determined by different sensors are represented with a solid line, airborne data 2002: crosses,  $n=6$ , FOY SeaWiFS 2002 dataset: solid triangle,  $n=10$ , PEGAU SeaWiFS 2003: solid circle,  $n=6$ , CARDER in situ shipboard: open circles,  $n=33$ , (b) relationship between field chlorophyll measurements ( $chl_{FOD}$ ) and calculated chl values using OC2d ( $chl_{FODest}$ ), 1:1 curve between observations is indicated with a solid line.

also reported more accurate chl estimates than ours using OC2d ( $RMSE_{\log_{10}}=0.235$ ). However, their results are not strictly comparable to ours since OC2d was originally developed with

Table 3  
Performance of SeaWiFS band-ratio remote-sensing algorithms to estimate chlorophyll  $a$  concentration (chl) in the first optical depth of Alaskan coastal waters

Algorithm	$\log R$	$N$	$R^2$	$RMSE_{\log_{10}}$	$\epsilon_{lr}$
OC2a	$\log(R_{rs}(412)/R_{rs}(553))$	14	0.69	0.41	1.09
OC2b	$\log(R_{rs}(443)/R_{rs}(553))$	14	0.81	0.29	0.71
OC2	$\log(R_{rs}(491)/R_{rs}(553))$	14	0.63	0.33	0.85
OC2d	$\log(R_{rs}(509)/R_{rs}(553))$	14	0.97	0.26	0.64

Empirical chl models proposed by O'Reilly et al. (1998), and based on SeaBAM (SeaBAM, SeaWiFS Bio-optical algorithm Mini-workshop) dataset. The general formulation for each band-ratio is a modified cubic polynomial function:  $chl=10^{(a_0+a_1 \cdot R+a_2 \cdot R^2+a_3 \cdot R^3)+a_4}$ , where  $a_0, a_1, a_2, a_3, a_4$  are regression coefficients obtained from Table 7 (O'Reilly et al., 1998).  $\log R$ : log-transformed band-ratio,  $N$ : number of validation points,  $R^2$ : coefficient of determination with intercept=0.0 and slope=1.0,  $RMSE_{\log_{10}}$ : root mean square error in  $\log_{10}$  scale,  $\epsilon_{lr}$ : linearized error between derived and true chl values.

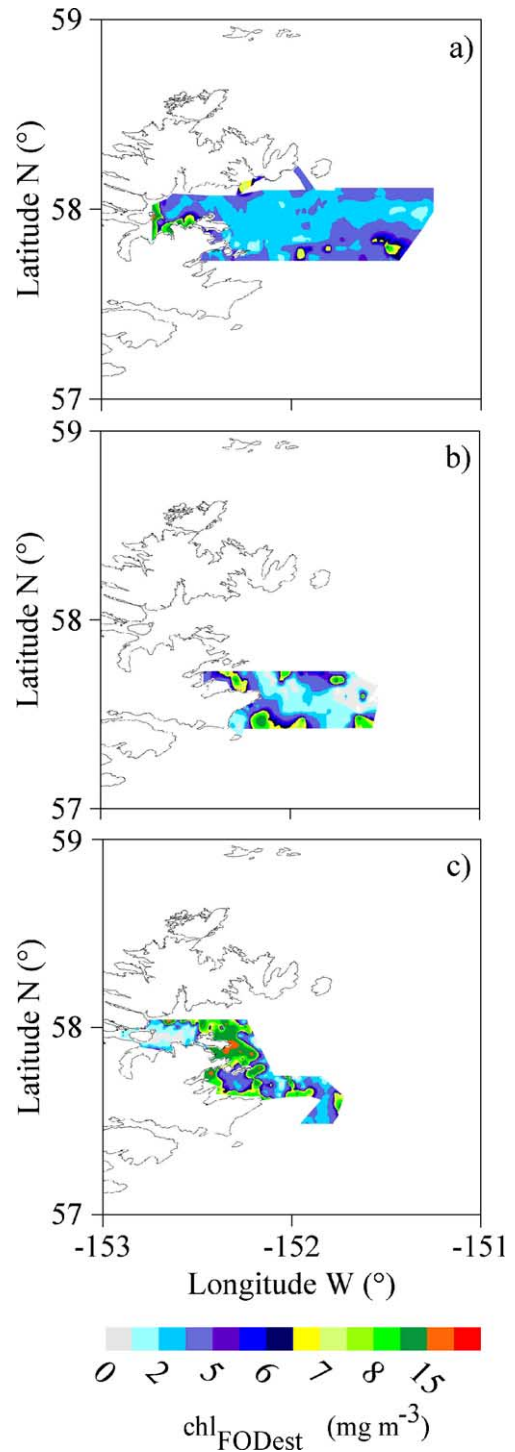


Fig. 5. Horizontal distributions of estimated chlorophyll concentration at the first optical depth during summer 2002. (a) 27 July, (b) 28 July, (c) 17 August.  $chl_{FODest}$ : estimated chlorophyll  $a$  concentration from airborne  $R_{rs}$  data and using OC2d.

global data (SeaBAM, SeaWiFS Bio-optical algorithm Mini-workshop), thus it was not tuned to particular regions such the NGOA. Furthermore, SeaBAM dataset contains very little data from polar regions and chl measurements above  $8 \text{ mg m}^{-3}$ . For the whole SeaBAM dataset ( $chl=0.02\text{--}32.8 \text{ mg m}^{-3}$ ), O'Reilly et al. (1998) also stated that maximum band-ratio algorithm (OC4) has a superior performance ( $RMS=0.156$ ,

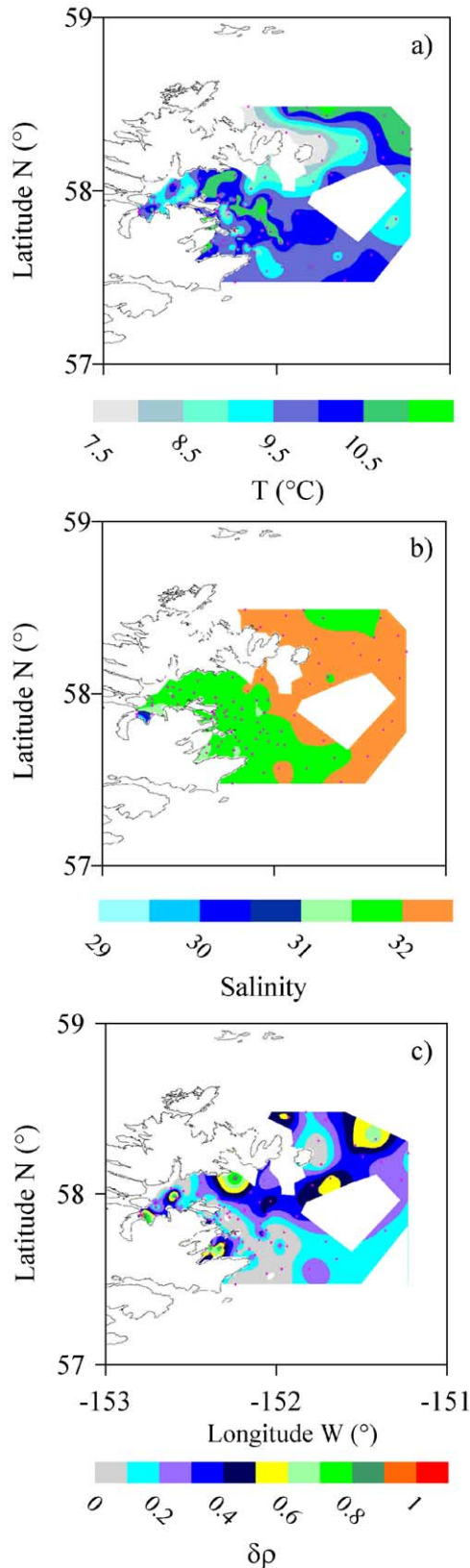


Fig. 6. Horizontal distribution of ancillary hydrographic information during summer 2002. (a) temperature, (b) salinity, (c) water column stratification.

$R^2=0.932$ ) to retrieve chl values over OC2a, OC2b, OC2 and OC2d. OC4 is a modified cubic polynomial model that finds the maximum band-ratio between  $R_{rs}(443)/R_{rs}(555)$ ,

$R_{rs}(490)/R_{rs}(555)$ , and  $R_{rs}(510)/R_{rs}(555)$ . Based on our dataset, OC4 had more uncertainty to predict chl<sub>FOD</sub> ( $RMSE_{\log_{10}}=0.27$ ,  $\epsilon_{\tau}=0.66$ ,  $n=14$ ) with respect to OC2d even though it worked better than remaining band-ratios algorithms tested in this study. Ability of OC4 to fairly estimate chl during summer 2002 surveys was not surprising given that most of reflectance spectra presented a maximum at 490 nm (Fig. 2a). In spite of its potential for NGOA, OC4 is a more demanding model than OC2d because it requires accurate atmospheric corrections in four bands instead of two (O'Reilly et al., 1998).

The band-ratio  $R_{rs}(510)/R_{rs}(555)$  was also a better predictor of chl in NGOA waters compared to those using

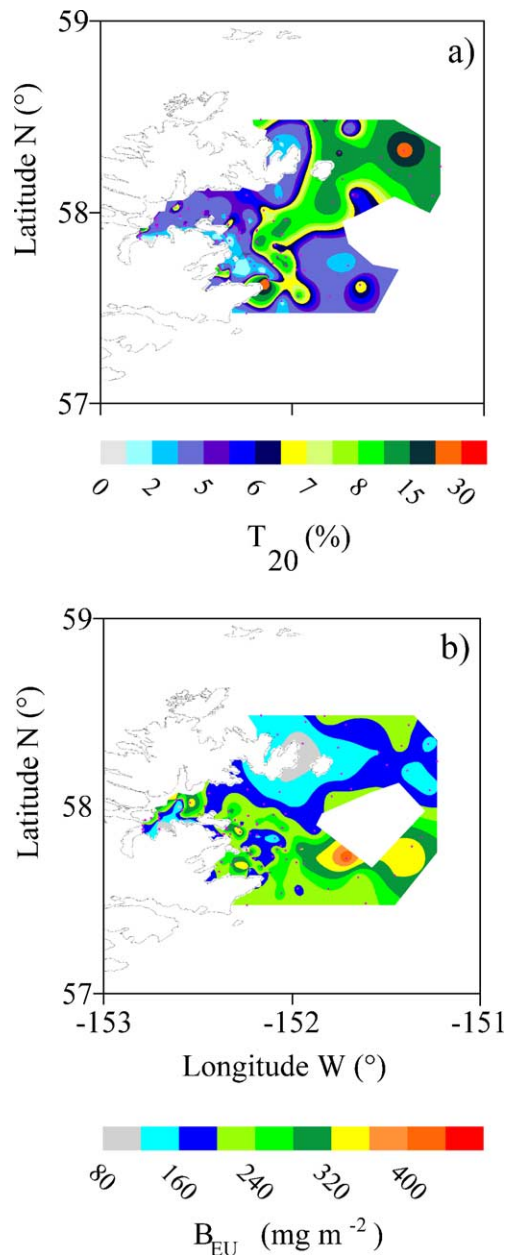


Fig. 7. Horizontal distribution of ancillary optical and biological information during summer 2002 (a) PAR transmission between 0 and 20 m, (b) integrated chl throughout the euphotic zone ( $B_{EU}$ ).

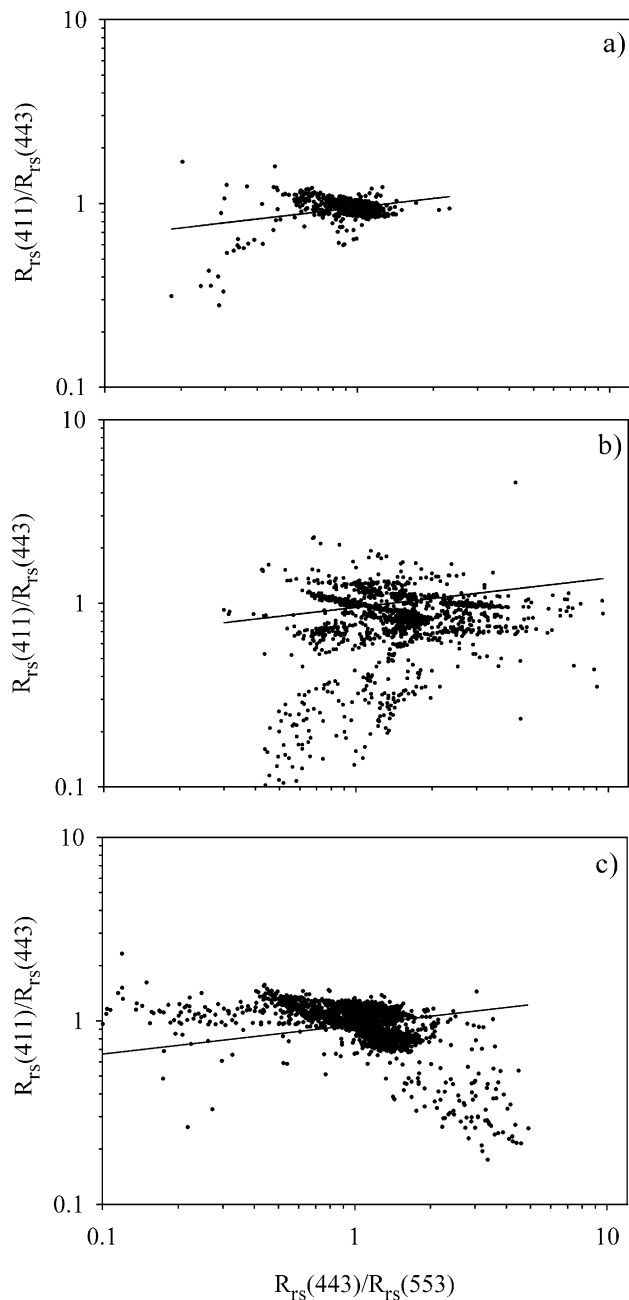


Fig. 8. Numerical filter for detecting waters with different gelbstoff content in coastal waters of Afgonak/Kodiak shelves. (a) 27 July, (b) 28 July, (c) 17 August 2002. The solid line in each panel represents the case I filter:  $R_{rs}(412)/R_{rs}(443) = 0.95 [R_{rs}(443)/R_{rs}(555)]^{0.16}$ . Gelbstoff enrichment and/or phytoplankton cells with significant packaging effects characterize dots below this line.

shorter wavelengths because it was less influenced by non-phytoplankton constituents (e.g. gelbstoff) that absorb light very strongly in the blue spectra ( $\lambda < 500$  nm) (Sathyendranath et al., 2004), and pigment-packaging effects (Kahru & Mitchell, 1998). For this reason, chl band-ratio and spectral-curvature relationships with wavelengths shorter or equal to 490 nm did not work very well in this study. In a fjord-like embayment characterized by gelbstoff-rich waters, Sathyendranath et al. (2004) used an airborne band-ratio algorithm based on  $R_{rs}(510)/R_{rs}(550)$  and  $R_{rs}(620)/R_{rs}(550)$  values to

estimate chl variability ( $3\text{--}22 \text{ mg m}^{-3}$ ). In coloured waters of Baltic Sea, Darecki et al. (2003) reported satellite-derived  $R_{rs}(550)/R_{rs}(590)$  as the most statistically significant algorithm to estimate chl values between ( $1$  and  $50 \text{ mg m}^{-3}$ ). Although no gelbstoff measurements were done during July–August 2002, the gelbstoff/packaging effect numerical filter (Eq. (11)) suggested a significant contribution ( $\sim 50\%$  of the stations) of humic substances/packaging effect to short-wave light attenuation. Important sources of gelbstoff in NGOA waters during summer are rivers (Royer, 1979). These freshwater inputs, originated by glacier/snow melting and sporadic runoff events, are enriched in colored substances when they cross anoxic–acidic ponds (muskeg meadows) rich on organic matter (e.g. wood detritus) (Terschak, 2002). Vertical mixing (inshore) and biological production (offshore) cannot be ruled out as additional sources of gelbstoff during 2002 surveys (Pegau, 2002). Glacier plumes not influenced by muskeg meadows are low in humic substances even though they can still contribute significantly to light attenuation at shorter wavelengths (412–490 nm) since they are rich in suspended fine-sediment (Curran et al., 2004; Pegau, 2002). Based on chl estimations without gelbstoff (semianalytical algorithm, Carder et al., 1999) (data not shown) pigment-packaging also appeared to be in this study a major factor affecting band-ratio and spectral-curvature relationships at wavelengths below 500 nm.

Another limitation of using shorter wavelengths ( $\lambda < 500$  nm) to estimate chl in NGOA waters was their shallow penetration along the vertical. This fact was particularly disadvantageous in NGOA waters during summer since maximum chl values were typically situated below the detection limit of blue  $R_{rs}$  channels. In that regard, a green wavelength combination such OC2d was more efficient since it was able to reach deeper waters (mean first optical depth  $\sim 7$  m) where in most of the cases a maximum chl peak developed (mean depth  $\sim 9.3$  m). For this reason, in most cases  $B_{EU}$  variability had a fair agreement with  $chl_{FOD}$  horizontal distributions. In July–August, there is strong stratification across the shelf and typical chl vertical profiles have a subsurface maximum (Stabeno et al., 2004).

Despite the OC2d advantages with respect to the other algorithms tested, chl estimates were less reliable in near-shore waters ( $< 30$  m) due to the bottom interference on reflectance values. This effect is more pronounced between 550 and 620 nm and also depends on water-bottom optical properties (Lee et al., 2001). In this study changes in green and brown algae abundances, and variations in sediment composition were expected to be the main factors increasing  $R_{rs}(553)$  with respect to  $R_{rs}(510)$  values near the coast. For instance, dense beds of green and brown macroalgae, and sand–gravel bottom caused over-estimation  $chl_{FODest}$  values (Fig. 5c) around the eastern part of Long Island (Gulf of Alaska Coastal Imagery Site, CIRCA-EVOS, <http://imf.geo-coch.html>). On this particular day, bottom influence on total  $R_{rs}(553)$  received at the airborne sensor was also enhanced due to low tides ( $\sim 1$  m MLLW).

OC2d-derived  $chl_{FOD}$  values showed that most fertile waters were preferentially located at the entrance of the Bays (e.g.

Marmot Bay, Chiniak Bay) and over the N. Albatross Bank. These areas share similar hydrographic features such as intense vertical mixing and intrusions of relatively low salinity waters (Fig. 6b,c). Due to the spring phytoplankton bloom, nutrient concentrations during summer are depleted in shelf waters of NGOA except below the pycnocline (Stabeno et al., 2004). Diverse physical mechanisms have been invoked to explain vertical nutrient fluxes (e.g. tidal mixing, cross-shelf transport) (Stabeno et al., 2004). In addition to macronutrients (e.g. nitrates) injected from bottom waters (e.g. slope GOA water), land-derived freshwater inputs provide an ample supply of micronutrients (e.g. iron) (Stabeno et al., 2004). Combinations of both nutrient sources make possible higher rates of phytoplankton production and chlorophyll synthesis (Stabeno et al., 2004). This fact may also explain why relative low chl<sub>FOD</sub> values were estimated over the troughs where a stronger stratification inhibits nutrient replenishment. Higher values of chl<sub>FOD</sub> estimated over N. Albatross Bank could also be caused by a higher residence time of phytoplankton cells with respect to troughs. Stabeno et al. (2004) found that shallows banks act as ‘particle traps’ based on trajectories of 50 satellite-tracked drifters. Since particles can stay for months over the banks (Stabeno et al., 2004), that corroborates the persistent pigment accumulations estimated in N. Albatross Bank.

In general terms, airborne reflectance measurements evidenced higher pigment levels in August with respect to July. The seasonal increase of chl from July to August is consistent with 1997–2001 SeaWiFS observations (Fig. 3b of Brickley & Thomas, 2004) and field observations over the Subarctic Pacific and Bering Sea (Banse & English, 1994). This phenomenon has been described as a response to relaxation of grazing pressure by micro and macro zooplankton (Harrison et al., 1999). Runoff due to rain and concomitant melting of snow and ice in coastal watersheds also stimulates phytoplankton growth (increasing *B*) from July to August because the introduction of micronutrients and increase of light levels by making shallower the upper mixed layer (Banse & English, 1994; Harrison et al., 1999; Stabeno et al., 2004). A positive effect of temperature on August chl build-up was certainly expected because the well known augmentation of microalgae growth with temperature (~2.0 fold with 10 °C increment) (Eppley, 1972). The use of airborne remote-sensing data was a valuable tool to estimate horizontal chl distributions in NGOA waters that avoided the limitations (low sun angles, cloudiness) of spaceborne sensors in high latitude environments. Unlike satellites, high-resolution aerial surveys also allowed spatial discrimination of small-scale *B* variations and its relationship with hydrographic features (e.g. banks vs. troughs pigment differences).

The approach used in this study to estimate chl distributions could be universal for Alaskan coastal waters even though algorithms must be tuned locally and for the same season before they can be useful for other coastal areas.

## Acknowledgements

We thank the captain and crew of the FV Laura of Kodiak for assistance during ship operations. Tim Veenstra at Airborne

Technologies Inc (Wasilla, Alaska) supported airborne missions. This study was supported by funds from the National Oceanic and Atmospheric Administration (National Marine Fisheries Service) supported Steller Sea Lion Research Initiative and Gulf Apex Predator–prey programs.

## References

- Banse, K., & English, D. C. (1994). Comparing phytoplankton seasonality in the eastern and western subarctic Pacific and western Bering Sea. *Progress in Oceanography*, 43, 235–287.
- Blough, N. V., Zafriou, O. C., & Bonilla, J. (1993). Optical absorption spectra of waters from the Orinoco River outflow: Terrestrial input of colored organic matter to the Caribbean. *Journal of Geophysical Research*, 98, 2271–2278.
- Brickley, P. J., & Thomas, A. C. (2004). Satellite-measured seasonal and inter-annual chlorophyll variability in the northeast Pacific and coastal Gulf of Alaska. *Deep-Sea Research Part II*, 51, 229–245.
- Brown, E. D., Churnside, J. H., Collins, R. L., Veenstra, T., Wilson, J. J., & Abnett, K. (2002). Remote sensing of capelin and other biological features in the North Pacific using LIDAR and video technology. *ICES Journal of Marine Science*, 59, 1120–1130.
- Campbell, J. W., & Esaias, W. E. (1983). Basis for spectral curvature algorithms in remote sensing of chlorophyll. *Applied Optics*, 22, 1084–1093.
- Carder, K. L., Chen, F. R., Lee, Z. P., & Hawes, S. K. (1999). Semianalytical moderate-resolution imaging spectrometer algorithms for chlorophyll a and absorption with bio-optical domains based on nitrate-depletion temperatures. *Journal of Geophysical Research*, 104(c3), 5403–5421.
- Curran, K. J., Hill, P. S., Milligan, T. G., Cowan, E. A., Syvitski, J. P. M., & Konings, S. M. (2004). Fine-grained sediment flocculation below the Hubbard Glacier meltwater plume. *Marine Geology*, 203, 83–94.
- Darecki, M., Weeks, A., Sagan, S., Kowalczyk, P., & Kaczmarek, S. (2003). Optical characteristics of two contrasting case 2 waters and their influence on remote sensing algorithms. *Continental Shelf Research*, 23, 237–250.
- Eltermann, L. (1968). *UV, visible, and IR attenuation for altitudes to 50 km, Report AFCRL-68-01653*. Bedford, MA: U.S. Air Force Cambridge Research Laboratory.
- Eppley, R. W. (1972). Temperature and phytoplankton growth in the sea. *Fishery Bulletin*, 70, 1063–1085.
- Gordon, H. R., Brown, J. W., Brown, O. B., Evans, R. H., & Clark, D. K. (1988). Exact Rayleigh scattering calculations for use with the Nimbus-7 coastal zone color scanner. *Applied Optics*, 27, 862–871.
- Gordon, H. R., & Clark, D. K. (1980). Atmospheric effects in the remote sensing of phytoplankton pigments. *Boundary-Layer-Meteorology*, 18, 299–313.
- Gordon, H. R., Clark, D. K., Brown, J. W., Brown, O. B., Evans, R. H., & Broenkow, W. W. (1983). Phytoplankton pigment concentrations in the middle Atlantic bight: Comparisons between ship determinations and coastal zone color scanner estimates. *Applied Optics*, 22, 20–36.
- Gordon, H. R., & McCluney, W. R. (1975). Estimation of the depth of sunlight penetration in the sea for remote sensing. *Applied Optics*, 14, 413–416.
- Gordon, H. R., & Morel, A. Y. (1983). *Remote assessment of ocean color for interpretation of satellite visible imagery: A review* (pp. 114). New York: Springer-Verlag.
- Grew, G. W. (1980). Real-time test of MOCS algorithm during superflux 1980. *NASA CP-2188* (p. 301).
- Harding, L. W., Itsweire, E. C., & Esaias, W. E. (1994). Estimates of phytoplankton biomass in the Chesapeake Bay from aircraft remote sensing of chlorophyll concentrations 1989–92. *Remote Sensing of Environment*, 49, 41–56.
- Harrison, P. J., Boyd, P. W., Varela, D. E., Takeda, S., Shiimoto, A., & Odate, T. (1999). Comparison of factors controlling phytoplankton in the NE and NW subarctic Pacific gyres. *Progress in Oceanography*, 43, 205–234.
- Hermann, A. J., Haidvogel, D. B., Dobbins, E. L., & Stabeno, P. J. (2002). Coupling global and regional circulation models in the coastal Gulf of Alaska. *Progress in Oceanography*, 53, 335–367.

- Hirons, A. C., Schell, D. M., & Finney, B. P. (2001). Temporal records of d13C and d15N in North Pacific pinnipeds: Inferences regarding environmental change and diet. *Oecologia*, *129*, 591–601.
- Kachel, N. B., Ladd, C., Mordy, C. W., Napp, J. M., & Stabeno, S. A. (2003). Nutrient supply to the GOA Shelf in summer: The role of troughs and shallow banks. *US Globec Symposium, Anchorage*.
- Kahru, M., & Mitchell, B. G. (1998). Spectral reflectance and absorption of a massive red tide off southern California. *Journal of Geophysical Research*, *103*(C10), 21601–21609.
- Lee, Z., Carder, K. L., Chen, R. F., & Peacock, T. G. (2001). Properties of the water column and bottom derived from Airborne Visible Infrared Imaging Spectrometer (AVIRIS) data. *Journal of Geophysical Research*, *106*, 11639–11651.
- Lee, Z., Carder, K. L., Steward, R. G., Peacock, T. G., Davis, C. O., & Mueller, J. L. (1996). Remote-sensing reflectance and inherent optical properties of oceanic waters derived from above-water measurements. *Ocean optics XIII*. Nova Scotia, Canada: Halifax.
- Loughlin, T. R., & York, A. E. (2000). An accounting of the sources of Steller sea lion, *Eumetopias jubatus*, mortality. *Marine Fisheries Review*, *62*, 40–45.
- Morel, A., & Bricaud, A. (1981). Theoretical results concerning light absorption in a discrete medium and application to the specific absorption of phytoplankton. *Deep-Sea Research. Part A*, *28*, 1357–1393.
- Neckel, H., & Labs, D. (1984). The solar radiation between 3300 and 12500. *A Solar Physics*, *90*, 205–258.
- O'Reilly, J. E., Maritorena, S., Mitchell, B. G., Siegel, D. A., Carder, K. L., & Garver, S. A., et al. (1998). Ocean color chlorophyll algorithms for SeaWiFS. *Journal of Geophysical Research*, *103*(c11), 24937–24953.
- Pegau, V. S. (2002). Inherent optical properties of the central Arctic surface waters. *Journal of Geophysical Research*, *107*(c10), 8035.
- Reinersman, P., & Carder, K. L. (1995). Monte Carlo simulation of the atmospheric point-spread function with an application to correction for the adjacency effect. *Applied Optics*, *34*, 4453–4471.
- Royer, T. C. (1979). On the effect of precipitation and runoff on coastal circulation in the Gulf of Alaska. *Journal of Physical Oceanography*, *9*, 553–563.
- Sathyendranath, S., Platt, T., Irwin, B., Horne, E., Borstad, G., & Stuart, V., et al. (2004). A multispectral remote sensing study of coastal waters off Vancouver Island. *International Journal of Remote Sensing*, *25*, 893–919.
- Stabeno, P. J., Bond, N. A., Hermann, A. J., Kachel, N. B., Mordy, C. W., & Overland, J. E. (2004). Meteorology and oceanography of the northern Gulf of Alaska. *Continental Shelf Research*, *24*, 859–897.
- Terschak, J.A. (2002). Phenanthrene adsorption by melanoidins and marine humic acids. PhD. Dissertation, University of Alaska Fairbanks.
- Trites, A. W., & Donnelly, C. P. (2003). The decline of Steller sea lions *Eumetopias jubatus* in Alaska: A review of the nutritional stress hypothesis. *Mammal Review*, *33*, 3–28.
- Trites, A. W., Miller, A. J., Maschner, H. D. G., Alexander, M. A., Bograd, S. J., Calder, J. A., Capotondi, A., Coyle, K. O., DiLorenzo, E., Finney, B. P., Gregr, E. J., Grosch, C. E., Hare, S. R., Hunt, G. L., Jahncke, J., Kachel, N. B., Kim, H. -J., Ladd, C., Mantua, N. J., Marzban, C., Maslowski, W., Mendelssohn, R., Neilson, D. J., Okkonen, S. R., Overland, J. E., Reedy-Maschner, K. L., Royer, T. C., Schwing, F. B., Wang, J. X. L. & Winship, A. J. in press. Bottom-up forcing and the decline of the Steller sea lions in Alaska: Assessing the ocean climate hypothesis. *Fisheries Oceanography*, 00,000–000.
- Venrick, E. L., & Hayward, T. L. (1984). Determining chlorophyll on the 1984 CalCOFI surveys. *CalCOFI Reports*, *25*, 74–79.
- Wessel, P., & Smith, W. H. F. (1996). A global, self-consistent, hierarchical, high-resolution shoreline database. *Journal of Geophysical Research*, *101*, 8741–8743.
- Wynne, K., & Foy, R. J. (2002). Is it food now? Gulf apex predator–prey study. In D. DeMaster, & S. Atkinson (Eds.), *Steller sea lion decline: Is it food II* (pp. 49–52). University of Alaska Sea Grant.